

Review

# An Overview on Graphene-Metal Oxide Semiconductor Nanocomposite: A Promising Platform for Visible Light Photocatalytic Activity for the Treatment of Various Pollutants in Aqueous Medium

Soumen Mandal <sup>1,†</sup>, Srinivas Mallapur <sup>2,†</sup>, Madhusudana Reddy <sup>2</sup>, Jitendra Kumar Singh <sup>3</sup>, Dong-Eun Lee <sup>4,\*</sup> and Taejoon Park <sup>5,\*</sup>

<sup>1</sup> Intelligent Construction Automation Center, Kyungpook National University, 80 Daehak-ro, Buk-gu, Daegu 41566, Korea; sou.chm@gmail.com

<sup>2</sup> Department of Chemistry, REVA University, Kattigenahalli, Yelahanka, Bangalore 560024, Karnataka, India; seenuseenum@gmail.com (S.M.); madhusudana.mb@reva.edu.in (M.R.)

<sup>3</sup> Innovative Durable Building and Infrastructure Research Center, Department of Architectural Engineering, Hanyang University, 1271 Sa3-dong, Sangnok-gu, Ansan 15588, Korea; jk200386@hanyang.ac.kr

<sup>4</sup> School of Architecture, Civil, Environment, and Energy, Kyungpook National University, 1370, Sangyegk-Dong, Buk-Gu, Daegu 702701, Korea

<sup>5</sup> Department of Robotics Engineering, Hanyang University, 55 Hanyangdaehak-ro, Ansan, Gyeonggi-do 15588, Korea

\* Correspondence: dolee@knu.ac.kr (D.-E.L.); taejoon@hanyang.ac.kr (T.P.); Tel.: +82-3140-05291 (T.P.)

† Equal contribution.

Received: 9 October 2020; Accepted: 12 November 2020; Published: 17 November 2020



**Abstract:** Graphene is one of the most favorite materials for materials science research owing to its distinctive chemical and physical properties, such as superior conductivity, extremely larger specific surface area, and good mechanical/chemical stability with the flexible monolayer structure. Graphene is considered as a supreme matrix and electron arbitrator of semiconductor nanoparticles for environmental pollution remediation. The present review looks at the recent progress on the graphene-based metal oxide and ternary composites for photocatalysis application, especially for the application of the environmental remediation. The challenges and perspectives of emerging graphene-based metal oxide nanocomposites for photocatalysis are also discussed.

**Keywords:** graphene oxide; metal oxides; semiconductor; photocatalysis; dyes

## 1. Introduction

Graphene is a 2-D material composed of layers of carbon atoms crammed into a honeycomb network and has become an escalating star on the prospect of materials science in the past many years [1–3]. Graphene can be used to produce 0-D fullerene, 1-D and 3-D graphitic carbon nanotubes that had been intensively studied for the last ten years [4,5]. Graphene exhibits enthralling assets such as extraordinary conductivity, maximum surface-area-to-volume ratio, a fluorescence-quenching competence by electron or energy-allocation, a quantum Hall effect at room temperature, a bipolar electric field effect laterally with the surface conduction of charge carriers and a tunable band gap [6,7]. Narrow band gap metal oxides are of great interest, due to their efficient utilization of solar energy which signifies an auspicious technology to resolve the global energy and eco-friendly challenges [5,8–10].

Furthermore, graphene sheets decorated with metal oxide nanoparticles exhibit the outstanding properties because of the synergetic effect between them [11].

The growth of graphene-based composites provides a significant milestone to multiply the application enactment of metal oxide nanomaterials in photocatalysis, as the hybrids have adaptable and suitable properties with superior performances over the individual oxide nanomaterials. With keeping this in mind, considerable efforts have been made on decorating graphene with metal oxides [12]. Graphene-based materials have also been used as the catalyst in the reactions pertaining to environmental remediation [13]. Graphene oxide-based (GO-based)/reduced graphene oxide-based (rGO-based) materials are used as photocatalysts for pollutant abatement [14–17].

In this context, focusing on the recent developments, an attempt is made in the present review to discuss the advantages and disadvantages of the composite in comparison with pristine graphene.

## 2. Photocatalysis

Different metal oxides-GO/rGO composites, their photocatalytic activities and synthesis process are discussed in the following sections as well as in Table 1. However, the photocatalytic performances of metal oxide-GO/rGO composite photocatalysts for the degradation of different pollutants are tabulated in Table 2.

### 2.1. Earth-Abundant Metal Oxide-GO/rGO Composites

#### 2.1.1. rGO-WO<sub>3</sub> Composites

rGO-WO<sub>3</sub> catalyst dosage has a substantial impression on the photocatalytic activity. The finest Sulfamethoxazole (SMX) removal efficacy was achieved when rGO-WO<sub>3</sub>-200 loading was 1.0 g L<sup>-1</sup>, and this study demonstrated that the dosage of the catalyst is crucial for the photocatalytic activity. SMX degradation over rGO-WO<sub>3</sub>-200 was significantly influenced by neutral pH and displayed the pre-eminent process [18]. Photodegradation of naphthol-1 by rGO-WO<sub>3</sub>-nanocomposite and WO<sub>3</sub> was achieved by 84% and 40% respectively, attributed to the larger specific surface area and lower band gap energy [19]. Outcomes suggested that the presence of rGO in the nanocomposite enabled the electron transfer [19]. The enhanced photocatalytic activity was due to the synergistic effect between WO<sub>3</sub> and rGO sheets and suppressing the electron-hole pair recombination in the WO<sub>3</sub>-rGO nanocomposite [6]. WO<sub>3</sub>/GO composites revealed an enhanced photocatalysis under the visible light, which was two-folds of pure WO<sub>3</sub> that reduced the recombination of the photogenerated electron-hole pairs and increased the visible light absorption efficiency [20].

#### 2.1.2. rGO-Co<sub>3</sub>O<sub>4</sub> Composites

Co<sub>3</sub>O<sub>4</sub>/rGO composite exhibits better photocatalytic activity in a low concentration of Methyl Orange (MO). The higher stocking dose of Co<sub>3</sub>O<sub>4</sub> on Co<sub>3</sub>O<sub>4</sub>/rGO contributes more on the activity [21]. Degradation of organic dyes depicted by photocatalytic experiments where GO acts as a supporting material and active co-catalyst, which decreases the band gap of  $\alpha$ -MoO<sub>3</sub> from 2.82 to 2.51 eV [22]. This synthesized hybrid can be used for visible-light-induced photocatalysis. Co<sub>3</sub>O<sub>4</sub>-rGO hybrids were reported to completely oxidize 20 mg/L phenol in 20 min at 25 °C. Origination of sulfate radicals via Co<sub>3</sub>O<sub>4</sub>-mediated activation of peroxymonosulfate (PMS) is responsible for this catalytic effect [23]. The Co<sub>3</sub>O<sub>4</sub>/N-doped graphene hybrid exhibits similar catalytic activity but superior stability to Pt, in alkaline solutions. This unusual catalytic activity arises from synergetic chemical coupling effects between Co<sub>3</sub>O<sub>4</sub> and graphene [23].

#### 2.1.3. GO/rGO-TiO<sub>2</sub> Composites

A systematic investigation on the photocatalytic properties of TiO<sub>2</sub>-GO nanocomposites was examined with different ratios of graphene additions and it was found that higher amount of graphene addition decreased the photocatalytic activity [24]. Liquid-phase degradation of dyes over the TiO<sub>2</sub>-GO

photocatalyst showed the similar occurrence. This study demonstrated that TiO<sub>2</sub>-GO cannot offer truly new visions into the assembly of TiO<sub>2</sub> carbon composite as high-performance photocatalysts. The TiO<sub>2</sub> particles were found to be in anatase phase and a narrow size distribution was dispersed on the surface of graphene sheets uniformly [25]. A comparison of photoluminescence spectra between TiO<sub>2</sub> and G-TiO<sub>2</sub> was reported with different reaction times, as shown in Figure 1. In this figure, the inset is the amplificatory image of the area in the range of 300 to 500 nm which demonstrates the quenching extent in relation with the reaction time in the Graphene-TiO<sub>2</sub> [26]. TiO<sub>2</sub> (P25)-rGO composite was found to be the most proficient photocatalyst for the degradation of Methylene Blue (MB) and the optimum mass ratio was found to be 1/0.2 [14]. Comparison has revealed that the P25-rGO composite has additional effectiveness compared to the P25-CNT (carbon nanotubes) composite (Figure 2).

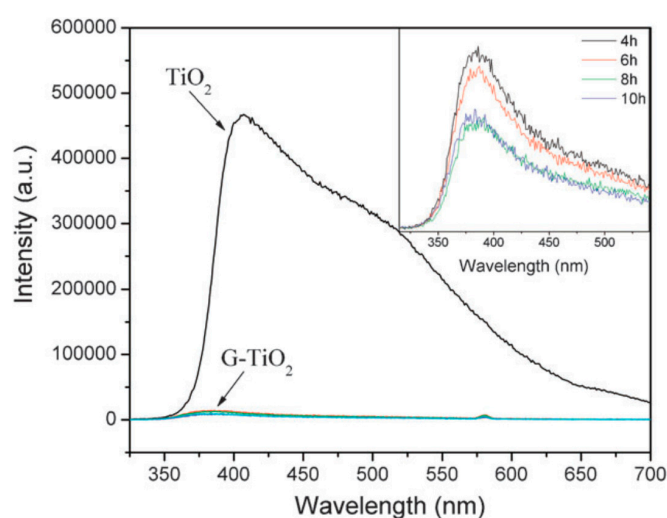


**Figure 1.** Photoluminescence spectra of TiO<sub>2</sub> and G-TiO<sub>2</sub> composite with various reaction times. The inset shows amplificatory image (300 to 550 nm) [26].

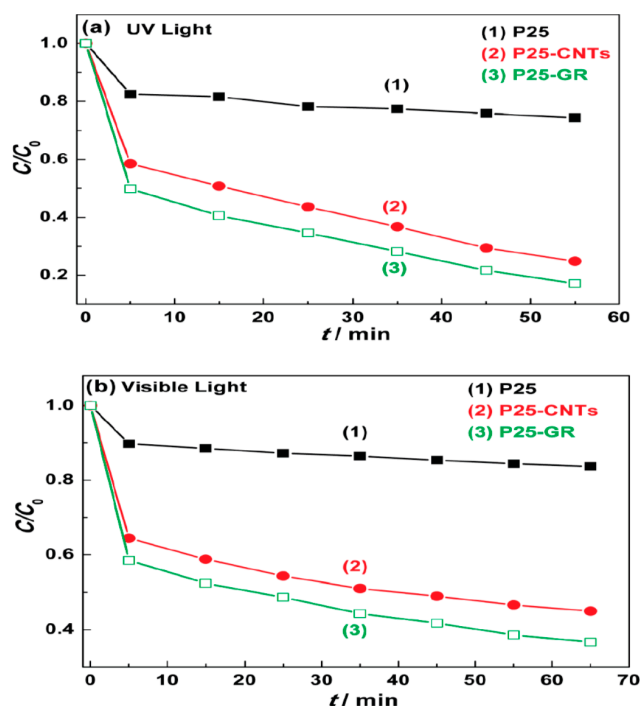


**Figure 2.** Degradation of Methylene Blue under (a) UV and (b) visible light ( $\lambda > 400$  nm) over (1) P25, (2) P25-carbon nanotubes (CNTs), and (3) P25-GR photocatalysts, respectively [14].

Graphene-loaded TiO<sub>2</sub> films were reported to be highly conductive and transparent; remarkably, graphene/TiO<sub>2</sub> films exhibited super hydrophilicity in a short time even under a white fluorescent light bulb. Higher photocatalytic activity owed to its efficient charge separation and electrons injection from the conduction band of TiO<sub>2</sub> to graphene [27].

The higher photocatalytic performance was observed in TiO<sub>2</sub>-graphene oxide composite due to the formation of both  $\pi$ - $\pi$  conjugations between dye molecules and aromatic rings. The photocatalytic property was reported to be higher with the higher content of the graphene oxide. Furthermore, ionic interactions between MB and functional groups of GO on the surfaces of carbon-based nanosheets was also the reason considered for the superior property [28]. Improving graphene oxide (IGO) in strong acidic condition was reported to enhance the chemical interaction between TiO<sub>2</sub> and graphene sheets [29]. This study showed that IGO can react with Ti(OH)<sub>x</sub> to form graphene/TiO<sub>2</sub> composite in situ, with complete and near coverage of Ti-C and Ti-O-C carbonaceous bonds at the graphene/TiO<sub>2</sub> interface. Higher photocatalytic activity shown by graphene/TiO<sub>2</sub> due to effective charge transfer imparts under visible light and GO forms chemical bonds at the interface [29].

Photocatalytic experiments using sacrificial hole and radical scavenging agents demonstrated that the photogenerated holes are the main reason for the degradation of diphenhydramine (DP), both under UV and visible light. In this report, photoluminescence studies revealed discrete appearing of the GO photoluminescence under visible light and near infrared laser excitation. Hence, it was conferred that GO acts as either an electron acceptor or donor of TiO<sub>2</sub> under UV/visible light [30].

Nitrogen-doped P90 TiO<sub>2</sub> (N-P90), nitrogen-doped reduced graphene oxide (N-rGO), as well as their composites were studied for the photocatalytic activity. N-P90/N-rGO showed enhanced photocatalytic activity, and in the presence of this composite, around 80% MB was degraded by visible light irradiation in 160 min. Enhanced photocatalytic performance is observed in N-P90/N-rGO composites for degradation of MB due to photo-induced and electronic interaction between TiO<sub>2</sub> and graphene. Comparison of degradation efficiency of MB under visible light irradiation by P90 TiO<sub>2</sub>, N-P90, and N-P90/rGO is presented in Figure 3 [31]. It is reported that the rGO or N-rGO in the composite enables the separation of electrons and holes by performing as electron trapping/de-trapping under visible light [31]. Ultrafine TiO<sub>2</sub> nanofibers (~10 nm diameters) were synthesized from electrospun rice-shaped TiO<sub>2</sub> and potassium titanate was achieved from rice-shaped TiO<sub>2</sub>. The surface area was increased by 2.5 times after the nanofiber formation of TiO<sub>2</sub>. The results showed that the photodegradation of MO was found to be higher than bare TiO<sub>2</sub> (P-25) nanoparticles [32]. GO/TiO<sub>2</sub> of different composition ratios were tested and the formulation of catalyst with 1.2 times higher photocatalytic activity than commercial photocatalyst was reported. This catalyst was able to degrade 3 mg/L MB over 10 consecutive cycles with nominal loss in photocatalytic efficacy. Graphene plays a generous part in obstructing the accretion of TiO<sub>2</sub> grains upon calcination at high temperature [33]. A set of reduced graphene oxide-TiO<sub>2</sub> (rGO-TiO<sub>2</sub>) nanocomposites was synthesized and examined for the photocatalytic activity by decolorization of Rhodamine B dye (RhB) under UV light. In this study, various parameters, such as dye concentration, rGO content, catalytic dose, and pH, were optimized for the decolorization. The catalysts were found to be more active at natural pH of the dye under the UV-illumination for the degradation of RhB dye. The presence of H<sub>2</sub>O<sub>2</sub> and K<sub>2</sub>S<sub>2</sub>O<sub>8</sub> increased the decolorization. Further, addition of CO<sub>3</sub><sup>2-</sup> and Cl<sup>-</sup> ions decreased the dye degradation rate [34].

TiO<sub>2</sub> nanoparticle-attached graphene/carbon composite nanofibers (TiO<sub>2</sub>-CCNFs) were synthesized and reported as highly active photocatalysts for photocatalytic degradation of MB under the irradiation of visible light. Graphene was suggested to play the role of an electron acceptor and a photosensitizer, resulting in a higher photodegradation rate and reduced electron-hole pair recombination. CNFs having high surface also improved the photocatalytic activity of TiO<sub>2</sub> [35].

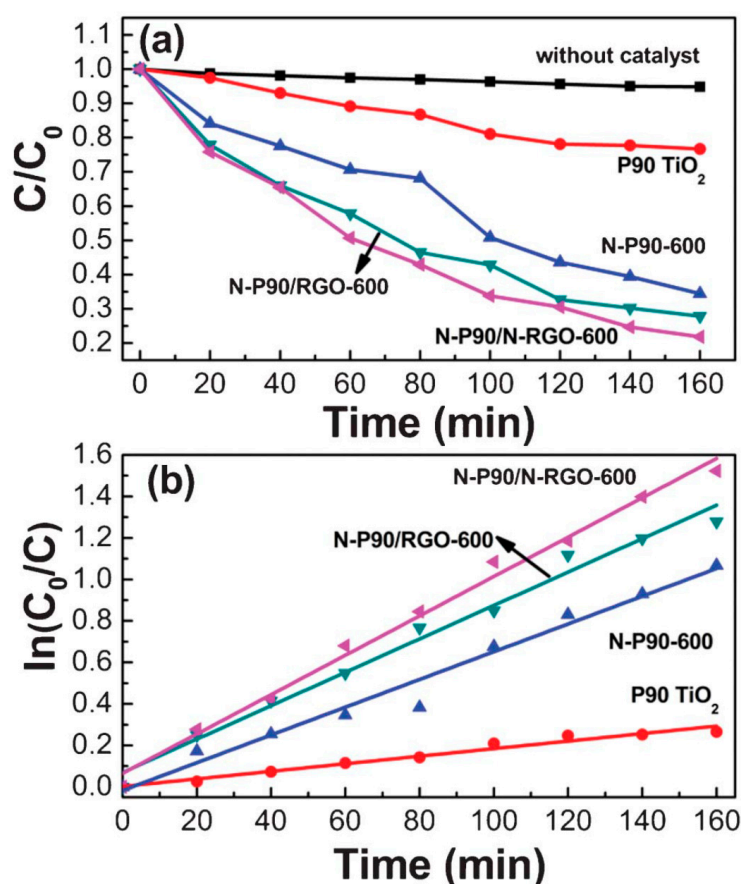


**Figure 3.** (a,b) Degradation of MB under visible light irradiation by P90 TiO<sub>2</sub>, N-P90-600, N-P90/reduced graphene oxide (rGO)-600, N-P90/N-rGO-600, and without catalyst [31].

#### 2.1.4. GO/rGO-ZnO Composite

An effective scalable method was developed to make nanocomposites of functional graphene sheets (FGS)/ZnO. In this study, poly (vinyl pyrrolidone) (PVP) component was reported to play a crucial role for loading of ZnO nanoparticles onto FGS by connecting Zn ions on the carbon materials and promoting ZnO nucleation and crystal growth in the precursor-prepared route. Further, FGS/ZnO composite was evaluated for photocatalytic activity and was found to be applicable for a number of environmental issues [36]. ZnO/rGO nanocomposite was used as a photocatalyst for the removal of MB. Observations showed that the efficiency of the photocatalyst activity of the ZnO nanoparticles was significantly increased by rGO [37].

The calcination atmosphere was found to affect the photocatalytic activity of the TiO<sub>2</sub>/graphene sheet (GS) (5%) composites for H<sub>2</sub> evolution from water splitting. This study demonstrated that beyond the critical content of GS (5%), photocatalytic activity was decreased by initiating electron-hole recombination centers. Calcination atmosphere was found to be important and better performance was observed for the samples calcined in nitrogen atmosphere [38].

The use of ZnO-graphene composites (Z-GC) was reported to remove dye from water due to the interaction between the graphene sheets and the ZnO nanoparticles [39]. rGO-ZnO (3.56%) showed higher photocurrent response and degradation of MB under illumination of UV light. Longer electron lifetime and the enhanced light absorption were verified by analytical and electrochemical technique (Figure 4) [40].

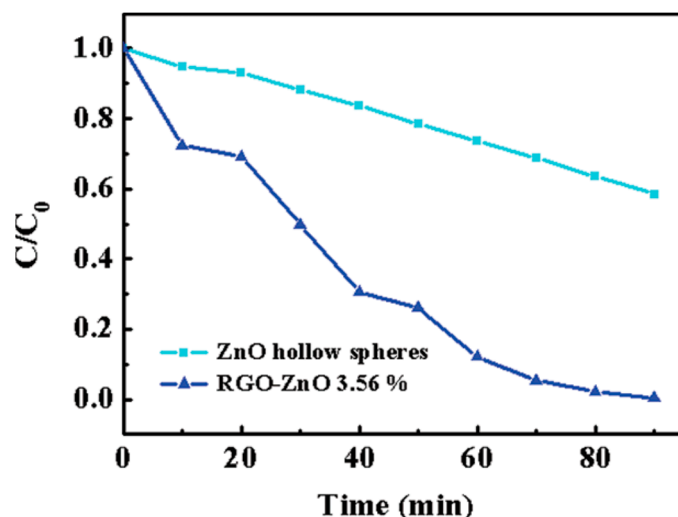


**Figure 4.** Photocatalytic activity of ZnO hollow spheres and rGO-ZnO 3.56% for the degradation of MB under UV illumination [40].

The ZnO/GO nanocomposite consisting of flower-like ZnO nanoparticles anchored on graphene-oxide. Further, photocatalytic efficiency of ZnO/GO composite progressed by annealing the product in N<sub>2</sub> atmosphere. The superior photocatalytic performance was due to the synergistic effect of the proficient electron inoculation and low charge carriers in the composite, where GO acted as an electron collector and transporter, leading to unceasing generation of reactive oxygen species for the degradation of MB [10]. Core-shell nanorods with ZnO core and ZnS-Bi<sub>2</sub>S<sub>3</sub> bi-component shell anchored on the rGO sheets were synthesized and reported to show a broad and strong photo-absorption in the visible region. These nanorods also manifested better photocatalytic activity for H<sub>2</sub> evolution from the glycerol-water mixtures. The superiority in performance is owing to the elevated light absorption and effective charge separation [41].

## 2.2. Bimetal Oxide-GO/rGO Composites

### 2.2.1. GO/rGO-CoFe<sub>2</sub>O<sub>4</sub> Composite

Connexion of the graphene suggestively progressed the photocatalytic performance of the CoFe<sub>2</sub>O<sub>4</sub> in which the graphene acts as a charge carrier to detain the delocalized electrons. Photocatalytic activity was explored with the variation of the dosage and dye concentration [42]. CoFe<sub>2</sub>O<sub>4</sub>-graphene hybrid materials (CFGHs) showed ferromagnetic behavior and enhanced photodegradation rate and amended adsorbing capacity due to the assimilation of graphene [43]. The photodegradation fallouts directed the visible light fascinating performance of the ternary photocatalysts and formation of the p-n junction between CoFe<sub>2</sub>O<sub>4</sub> and CdS. Escalation in the concentration of MB was observed as the irradiation time increased for CoFe<sub>2</sub>O<sub>4</sub> due to the desorption of MB during irradiation. G-CoFe<sub>2</sub>O<sub>4</sub>/CdS easily separated from aqueous solution in an external magnetic field, as seen from the digital photos of Gr-CoFe<sub>2</sub>O<sub>4</sub>/CdS after irradiation [44]. The CoFe<sub>2</sub>O<sub>4</sub>-rGO composite unveiled required photocatalytic performance with excellent recycling stability for the degradation of MB, RhB, and MO under visible-light irradiation [45].

CoFe<sub>2</sub>O<sub>4</sub>-rGO (CF-rGO) nanocomposites hold exceptional microwave absorbing properties and high photocatalytic activity for the degradation of various dyes under visible light irradiation [46]. 85 CF-15 rGO exposed admirable microwave absorption possessions with a Reflection Loss (RL) of 31.31 dB (99.94% absorption) at 9.05 GHz, with an 8.2–10.92 GHz effective bandwidth range. 75CF-25 rGO was found to be a good magnetically separable photocatalyst for the degradation of dyes, MO, MB, and RhB, under visible light irradiation emitted from a 100 W reading lamp [46]. The photocatalytic activity was found to be affected by the structural and optical properties and surface area of the samples [47].

CoFe<sub>2</sub>O<sub>4</sub>-3D TiO<sub>2</sub> nanocomposite showed an enhancement in the photodegradation of MB as compared to the commercial rutile-phase TiO<sub>2</sub> and the pure urchin-like TiO<sub>2</sub> (3D TiO<sub>2</sub>) microparticles. Results specified that the composite showed relatively consistent photocatalytic activity with slight degradation [48]. The photocatalytic activity of 75CF-25 rGO was found to be analogous and in some cases, superior, compared to the several reported rGO-CoFe<sub>2</sub>O<sub>4</sub> composites [46]. The photocatalytic activity of CF-RGO was increased with increasing rGO content in composites until 25 wt% of rGO, and degradation takes place around 60 min.

The photocatalytic degradation of short-chain chlorinated paraffin's over rGO/CoFe<sub>2</sub>O<sub>4</sub>/Ag under visible light ( $\lambda > 400$  nm) was investigated by in-situ Fourier transform infrared spectroscopy and the correlated mechanisms were suggested. Superficial degradation ratio of 91.9% over rGO/CoFe<sub>2</sub>O<sub>4</sub>/Ag was obtained under visible light illumination of 12 h, while only about 21.7% was obtained with commercial P-25 TiO<sub>2</sub> [49]. Increase of rGO caused an increase in the completion time of the photocatalysis. Degradation of MO diminished with increasing catalyst dose up to 500 mgL<sup>-1</sup>, and then, no noteworthy decrease of time was observed when more catalyst was added. Likewise, use of 2 mL of H<sub>2</sub>O<sub>2</sub> was found to be an optimum amount for the photocatalysis reaction (Figure 5) [46]. Photocatalytic activity of the rGO-CoFe<sub>2</sub>O<sub>4</sub> nanocomposites was queried for the degradation of 4-Chlorophenol (4-CP) under visible light illumination. Activity of rGO-CoFe<sub>2</sub>O<sub>4</sub> composite was seen in the occurrence of PMS (Figure 6) [50].

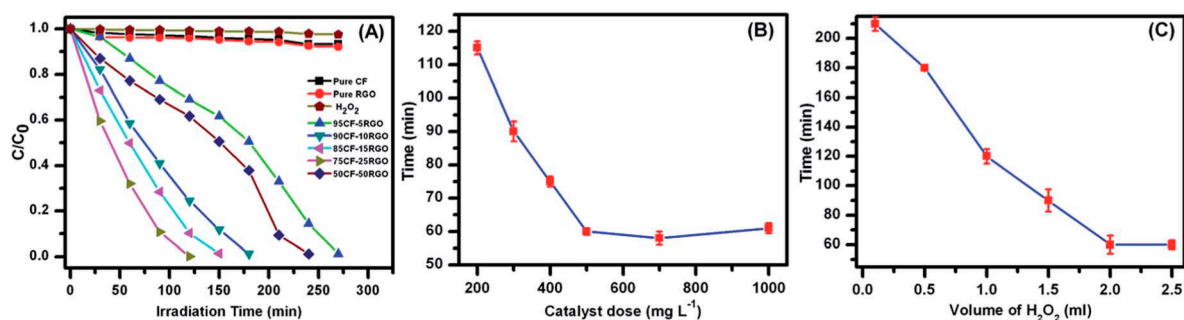


**Figure 5.** (A) Different catalysts for the degradation of Methyl Orange (MO) under visible light. (B) Catalyst dosage and (C) H<sub>2</sub>O<sub>2</sub> on the accomplishment time of photocatalysis reaction of MO catalyzed by 75CF-25RGO [46].

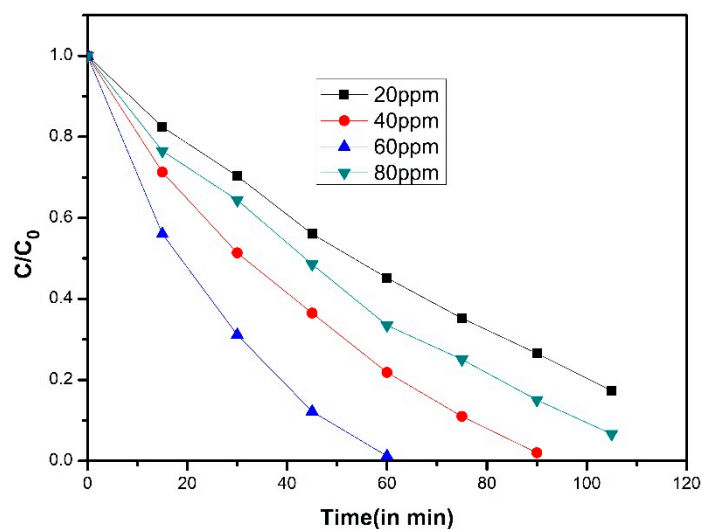


**Figure 6.** Plot of  $C/C_0$  vs. time in min for the degradation of 4-CP (10 ppm) with 100 mg of catalyst at various peroxymonosulfate (PMS) concentrations [50].

### 2.2.2. GO-rGO-ZnFe<sub>2</sub>O<sub>4</sub> Composite

Photocatalytic activity of ZnFe<sub>2</sub>O<sub>4</sub>-graphene catalyst demonstrated an important two-fold function as the photoelectrochemical degradation of MB and generation of hydroxyl radical for the decomposition of H<sub>2</sub>O<sub>2</sub> under visible light irradiation [51]. Graphene-ZnFe<sub>2</sub>O<sub>4</sub> photocatalyst facilitated the transport channels for photon-excited electrons from the surface of the catalyst. As a result, about 20 nm ZnFe<sub>2</sub>O<sub>4</sub> catalyst with a highly crystallized (311) plane confined in the graphene network exhibited an excellent visible-light-driven photocatalytic activity with an ultrafast degradation rate of  $1.924 \times 10^{-7} \text{ mol g}^{-1} \text{ s}^{-1}$  for MB [52].

The boosted photocatalytic activity of ZnFe<sub>2</sub>O<sub>4</sub>-rGO nanocomposite was shown due to the active restraint of the recombination of the photo-excited electron-hole pairs by rGO sheets and the generation of ·OH-free radical [11]. The photocatalytic activity of the nanocomposite examined under visible light, for the degradation of 17  $\alpha$ -ethinylestradiol (EE<sub>2</sub>) [50]. The pseudo rate constant of ZnFe<sub>2</sub>O<sub>4</sub>-Ag/rGO nanocomposite was higher by the factor of 14.6 and 5.6 times over its counterparts. Photosensitization effect was prevailed by good interaction ensuing in only 80% removal of EE<sub>2</sub> though humic acid [53]. rGO/ZnFe<sub>2</sub>O<sub>4</sub> composite exhibited the remarkable catalytic activity toward MB degradation; in the presence of H<sub>2</sub>O<sub>2</sub>, the activity enhanced, and the reaction followed a pseudo-first-order kinetics. The complete MB degradation observed at rGO/ZnFe<sub>2</sub>O<sub>4</sub> composites was attributed to the  $\pi$ - $\pi$  interaction, hydrogen bonding, and electrostatic interaction exerted between the rGO and ZnFe<sub>2</sub>O<sub>4</sub> [54].

### 2.2.3. GO/rGO-NiFe<sub>2</sub>O<sub>4</sub> and MnFe<sub>2</sub>O<sub>4</sub> Composites

NiFe<sub>2</sub>O<sub>4</sub>-GO (0.25) hetero-architecture demonstrated a considerable lesser emission intensity. Due to their competent electron-transport property, graphene sheets can deliberately reduce the fluorescence of NiFe<sub>2</sub>O<sub>4</sub> fixed on them. Kinetic results indicated that the rate-determining step is the adsorption course of MB [55]. In this study, NiFe<sub>2</sub>O<sub>4</sub>-GO (0.25) shows the best activity compared to other NiFe<sub>2</sub>O<sub>4</sub>-G composites (Figure 7). GO-NiFe<sub>2</sub>O<sub>4</sub> showed photo-Fenton reactions for organic contaminants in the presence of both H<sub>2</sub>C<sub>2</sub>O<sub>4</sub> and H<sub>2</sub>O<sub>2</sub> under visible light irradiation. The photochemical reduction of Fe<sup>3+</sup> ions by GO was a key step in inducing the Fenton process [56]. The superior photocatalytic is due to (I) high visible absorbance for charge carrier production, (II) the electrons captured by Au nanoparticles results in the fast separation, and (III) the strong surface plasmon resonance (SPR) of Au nanoparticles permit the generation of high concentration of charge carriers [57]. MnFe<sub>2</sub>O<sub>4</sub> catalyst is photocatalytically inactive. The noteworthy higher photocatalytic activity is due to the rGO, as the excellent conductivity in the MnFe<sub>2</sub>O<sub>4</sub> and graphene composite [58].

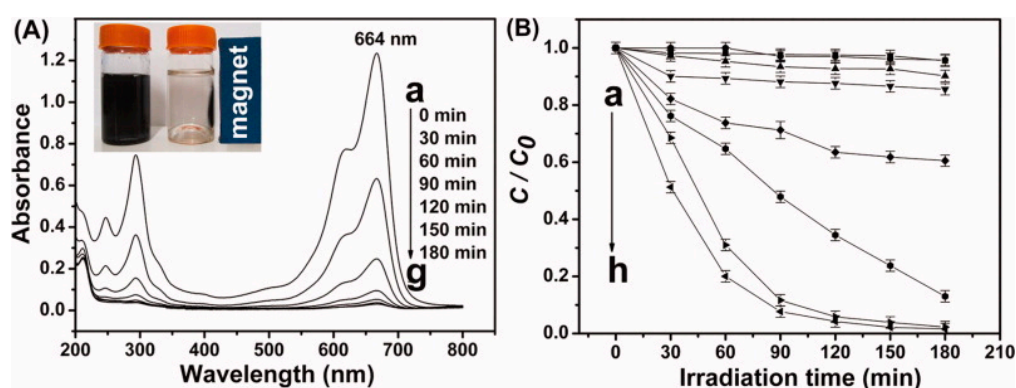


**Figure 7.** Absorption spectra of MB taken at various photocatalytic degradation times consuming NiFe<sub>2</sub>O<sub>4</sub>-GO (0.25) [55]. (A) The magnetic separation property of NiFe<sub>2</sub>O<sub>4</sub>-graphene nanocomposite is shown in the inset, (B) different catalysts and their photocatalytic degradation efficiency on MB: (a) pure NiFe<sub>2</sub>O<sub>4</sub>, (b) NiFe<sub>2</sub>O<sub>4</sub>-G(0.05), (c) NiFe<sub>2</sub>O<sub>4</sub>-G(0.10), (d) NiFe<sub>2</sub>O<sub>4</sub>-G(0.15), (e) NiFe<sub>2</sub>O<sub>4</sub>-G(0.20), (f) NiFe<sub>2</sub>O<sub>4</sub>-G(0.40), (g) NiFe<sub>2</sub>O<sub>4</sub>-G(0.30), and (h) NiFe<sub>2</sub>O<sub>4</sub>-G(0.25).

### 2.2.4. Other Composite Systems

RGO-Bi<sub>2</sub>WO<sub>6</sub> and 3D CNT-pillared rGO nanocomposites show outstanding photocatalytic performance for the degradation of dyes under visible light [59]. BiFeO<sub>3</sub>-graphene nanohybrids have a six times higher rate compared to BiFeO<sub>3</sub> for the degradation of Congo Red (CR) under visible light due to its combined effects of modulated band gap and covalent bonding between BiFeO<sub>3</sub> and graphene [60].

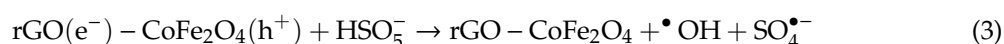
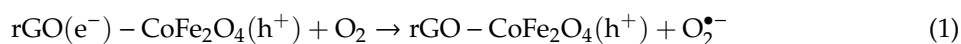
Photoluminescence studies of Nb<sub>3</sub>O<sub>7</sub>(OH)-RGO composite supported the suggested mechanism of charge separation and transport mechanism. A higher degradation rate was obtained using the nanocomposite prepared with a graphene loading of 3 mgmL<sup>-1</sup>, and when the rGO loading exceeded 3 mgmL<sup>-1</sup>, degradation efficacy diminished. This arose as extra rGO sheets gathered and stuck the absorption of incident light [61].

## 3. Photocatalytic Evaluation

Pristine TiO<sub>2</sub> and ZnO exhibited good photocatalytic activity in UV light due to their wide band gap. These two metal oxides are stable in aqueous conditions during photocatalysis. Further, coupling of graphene with TiO<sub>2</sub> and ZnO increases the photocatalytic activity due to increases in the photogenerated charge carriers. Metal oxides with magnetic properties of metal ferrites (MFe<sub>2</sub>O<sub>4</sub>) offer an added advantage as photocatalysts since they can be recovered by applying an external magnetic field after catalysis. Metal ferrites (MFe<sub>2</sub>O<sub>4</sub>, M = Co, Ni, Mn, Zn, etc.) materials are proven to be excellent candidates for visible light photocatalytic H<sub>2</sub> generation through water splitting. Recycling ability for metal ferrites are far better compared to nano semiconductors like TiO<sub>2</sub> and ZnO. MFe<sub>2</sub>O<sub>4</sub> is a class of semiconductor with narrow band gap, which exhibits characteristic visible light response, possess good photochemical stability, and exhibits excellent optical properties.

MFe<sub>2</sub>O<sub>4</sub> absorbs 42–45% of sunlight, whereas TiO<sub>2</sub> and ZnO absorbs 4% of sunlight. MFe<sub>2</sub>O<sub>4</sub> are efficient for the degradation of dye degradation and organic pollutant degradation compared to the other metal oxides (SnO<sub>2</sub>, CeO<sub>2</sub>, BaTiO<sub>3</sub>, and SrTiO<sub>3</sub>), with respect to the catalyst and the light source. In MFe<sub>2</sub>O<sub>4</sub> context, recombination of photogenerated charge carriers is the major limitation in semiconductor photocatalysis as it reduces the overall quantum efficiency. In order to enhance the photocatalytic activity, graphene material is coupled with MFe<sub>2</sub>O<sub>4</sub>, where the graphene channels the electrons. Comparison of degradation rate for various photocatalytic reaction systems is incongruous since the nature of catalyst and substrate pollutant molecules are different in each reaction. Ferrite nanoparticles have a strong magnetic property, which can be easily used for magnetic separation after photo-mineralization.

The photocatalytic efficiency depends on the ratio of the photogenerated charge-carrier transfer rate to the rate of electron-hole recombination. For composite structure, M<sup>2+</sup> ion easily bonds with oxygen by giving an electron and super oxide radical. This super oxide radical can oxidize the organic substrate molecule. The Fe<sup>3+</sup> ion and Fe<sup>2+</sup> ions can show photo-Fenton reactions in presence of in-situ-generated H<sub>2</sub>O<sub>2</sub>. This H<sub>2</sub>O<sub>2</sub> generates hydroxyl-free radicals, which are involved in the degradation of pollutants. Predicted mechanism for the rGO-CoFe<sub>2</sub>O<sub>4</sub> composite is shown in Equations (1)–(4).



rGO-BiO<sub>6</sub> composite shows better photocatalyst compared to other catalysts prepared from hydrothermal method (Table 1; Table 2). The enhanced photocatalytic activity could be endorsed to the negative shift in the Fermi level of graphene-Bi<sub>2</sub>WO<sub>6</sub> (G-BWO), decrease the conduction

band potential, and elevate migration efficiency of photo-induced electrons, which may restrain the charge recombination efficiently. Superior contact between  $\text{BiVO}_4$  and rGO scaffold subsidizes to photo-response augmentation compared to other electrochemical methods in the rGO- $\text{BiVO}_4$  composite.

**Table 1.** Photocatalysts and their typical synthetic methods used for the preparation from GO/rGO-supported composites.

Order	Photocatalyst	Preparation	References
<b>A. Hydrothermal method for the synthesis of GO/rGO-NCs photocatalyst</b>			
1	rGO- $\text{WO}_3$	$\text{Na}_2\text{WO}_4 \cdot 2\text{H}_2\text{O}$ and 0.05 g NaCl were dissolved in the above dispersion and kept stirring for 1 h. The pH was adjusted to 2 by using HCl solution.	[6]
2	rGO- $\text{WO}_3$	Preset amounts of $\text{Na}_2\text{WO}_4 \cdot 2\text{H}_2\text{O}$ (100, 200, and 400 mg, respectively) were dissolved in 10 mL above GO suspension. 5 mL 35% HCl was added slowly. Transferred to autoclave heated at 140 °C for 8 h.	[18]
3	rGO- $\text{Co}_3\text{O}_4$	GO dispersed into 24 mL of alcohol, sonicating for 60 min in an ultrasonic cleaner. Then, 0.2 M of $\text{Co}(\text{Ac})_2$ was added to the mixture followed by 1.2 mL of water, and continued to be stirred for 10 h at a temperature of 80 °C. The resulting solution was then transferred into a 40 mL autoclave for hydrothermal reaction at 150 °C for 3 h.	[21]
4	rGO- $\text{Co}_3\text{O}_4$	GO dispersed in the $\text{Co}(\text{C}_2\text{H}_3\text{O}_2)_2 \cdot 4\text{H}_2\text{O}$ . 10 mL with 28% ammonia solution were added to solution, and transferred into an autoclave for hydrothermal action at 180 °C for 12 h.	[23]
5	rGO/ $\text{ZnFe}_2\text{O}_4$ -Ag	The composite was synthesized by the co-precipitation of $\text{Zn}(\text{NO}_3)_2 \cdot 6\text{H}_2\text{O}$ , $\text{Fe}(\text{NO}_3)_3 \cdot 9\text{H}_2\text{O}$ , and $\text{AgNO}_3$ in the presence of the GO powder.	[53]
6	GO- $\text{NiFe}_2\text{O}_4$	GO in $\text{NiFe}_2\text{O}_4$ was dispersed in deionized water. Then, $\text{NiSO}_4 \cdot \text{H}_2\text{O}$ and $\text{FeCl}_3 \cdot 6\text{H}_2\text{O}$ (0.02 mol) were dissolved in 15 mL water. Transferred into autoclave and kept under high pressure.	[56]
7	GO- $\text{MnFe}_2\text{O}_4$	GO and 60 mL of ethanol with sonication for 1 h and $\text{Mn}(\text{NO}_3)_2$ solution and $\text{Fe}(\text{NO}_3)_3 \cdot 9\text{H}_2\text{O}$ were dissolved. The resulting mixture was transferred into a 100 mL Teflon-lined stainless-steel autoclave and heated to 180 °C for 20 h under autogenous pressure.	[58]
8	rGO- $\text{Bi}_2\text{WO}_6$	GO by using Hammer method GO was reduced by ethylene glycol. $\text{Bi}(\text{NO}_3)_3 \cdot 5\text{H}_2\text{O}$ was dispersed into 5 mL of 4 M nitric acid solution. $\text{Na}_2\text{WO}_4 \cdot 2\text{H}_2\text{O}$ was dissolved in 5 mL of de-ionized water and then $\text{Na}_2\text{WO}_4$ was added dropwise to the solution.	[59]
<b>B. Sol-gel method for the synthesis of GO/rGO-NCs photocatalysts</b>			
9	rGO- $\text{TiO}_2$	An aqueous solution of $\text{Ti}(\text{OH})_4$ was added into an aqueous suspension of GO.	[30]
10	rGO- $\text{ZnO}$	An aqueous solution of $\text{Zn}(\text{AcO})_2 \cdot 3\text{H}_2\text{O}$ was added into an aqueous suspension of GO.	[39]

Table 1. Cont.

Order	Photocatalyst	Preparation	References
<b>C. Solvothermal technique for the GO/rGO-NCs photocatalysts</b>			
11	GO/CoFe <sub>2</sub> O <sub>4</sub> /CdS	Gr-CoFe <sub>2</sub> O <sub>4</sub> nanohybrids were sonicated in 60 mL of ethylene glycol for 10 min. The cadmium source containing 0.1431 g of Cd(NO <sub>3</sub> ) <sub>2</sub> ·4H <sub>2</sub> O and 10 mL of ethylene glycol was added to the mixture containing Gr-CoFe <sub>2</sub> O <sub>4</sub> nanohybrids. The mixture of 0.0348 g of thiourea, 0.0514 g of PVP, and 10 mL of ethyleneglycol was transferred into the above mixture.	[44]
12	rGO-ZnFe <sub>2</sub> O <sub>4</sub>	GO dispersed in ZnO <sub>x</sub> (OH) <sub>y</sub> and FeO <sub>x</sub> solutions were put into a 50 mL autoclave.	[51]
<b>D. Colloidal method for the synthesis of GO/rGO-NCs photocatalyst</b>			
13	rGO-ZnFe <sub>2</sub> O <sub>4</sub>	C <sub>2</sub> H <sub>6</sub> O <sub>2</sub> solution is containing 2M FeCl <sub>3</sub> ·6H <sub>2</sub> O, and 1M ZnCl <sub>2</sub> was gradually added. Then, 1MCH <sub>3</sub> COONa was introduced into the solution and magnetically stirred for 1 h. Then, transferred to autoclave heated at 1800 °C.	[54]
<b>E. Thermal treatment for the synthesis of GO/rGO-NCs photocatalyst</b>			
14	rGO-WO <sub>3</sub>	Na <sub>2</sub> WO <sub>4</sub> ·2H <sub>2</sub> O was dissolved in 30 mL water. Then, nitric acid was added to the solution drop by drop until the precipitate was formed. Dried at 160 °C for 2 h and annealed at 500 °C for 5 h.	[19]
15	rGO-WO <sub>3</sub>	Na <sub>2</sub> WO <sub>4</sub> ·2H <sub>2</sub> O (0.5 g), H <sub>2</sub> C <sub>2</sub> O <sub>4</sub> (1 g), and Na <sub>2</sub> SO <sub>4</sub> (4 g) were added into subsequent solution and stirred for 3 h. The pH of the solution was maintained at 1.5 by adding 3M HCl and stirring was continued for 3 h. Then, transferred to autoclave maintained at 180 °C for 24 h.	[20]
16	FGS/ZnO	GO, Zn(NH <sub>3</sub> ) <sub>4</sub> CO <sub>3</sub> , and poly(vinyl pyrrolidone) as an intermediate to combine zinc with carbon material	[36]
<b>F. Ball-milling method for the synthesis of GO/rGO-NCs photocatalyst</b>			
17	rGO-CoFe <sub>2</sub> O <sub>4</sub>	Co (NO <sub>3</sub> ) <sub>2</sub> ·6H <sub>2</sub> O and of Fe (NO <sub>3</sub> ) <sub>3</sub> ·9H <sub>2</sub> O were added to GO (2.5 wt%). The pH is maintained 10	[45]
18	rGO-CoFe <sub>2</sub> O <sub>4</sub>		[45]
19	rGO-CoFe <sub>2</sub> O <sub>4</sub>		[45]
<b>G. Liquid phase deposition method for the synthesis of GO/rGO-NCs photocatalyst</b>			
20	rGO-TiO <sub>2</sub>	TiO <sub>2</sub> powder (P25, Degussa) was dispersed in deionized water and subsequently added to the graphene oxide solution	[28]
<b>H. Microwave irradiation method for the synthesis of GO/rGO-NCs photocatalyst</b>			
21	rGO-CoFe <sub>2</sub> O <sub>4</sub>	(Co(NO <sub>3</sub> ) <sub>2</sub> ·6H <sub>2</sub> O and Fe(NO <sub>3</sub> ) <sub>3</sub> ·9H <sub>2</sub> O and glucose as oxidizer and fuel. GO, nitrates, and glucose were added in water for 30 min ultrasonic treatment.	[43]
22	rGO-CoFe <sub>2</sub> O <sub>4</sub>		[43]
23	rGO-CoFe <sub>2</sub> O <sub>4</sub>		[43]
24	rGO/CoFe <sub>2</sub> O <sub>4</sub> /Ag	GO, AgNO <sub>3</sub> , and CoFe <sub>2</sub> O <sub>4</sub> were dissolved in deionized water and stirred for 2 h. Then, solution was further stirred for 2 h under the UV irradiation of a 22 W low-pressure mercury lamp. The product is washed with distilled water and ethanol in an oven at 60 °C for 12 h.	[49]
<b>I. In situ co-precipitation method for the synthesis of GO/rGO-NCs photocatalyst</b>			

Table 1. Cont.

Order	Photocatalyst	Preparation	References
25	rGO-ZnO	GO dispersed in aqueous solution containing Zn(CH <sub>3</sub> COO) <sub>2</sub> , DMSO, and H <sub>2</sub> O	[40]
<b>J. Annealing NH<sub>3</sub> atmosphere method for the synthesis of GO/rGO-NCs photocatalyst</b>			
26	rGO/N-TiO <sub>2</sub>	GO and 300 mg of P90 TiO <sub>2</sub> was added and stirred for 3 h. GO and P90 TiO <sub>2</sub> and a few drops of tetrabutyltitanate were added.	[31]

**Table 2.** Photocatalytic performances of GO/rGO-NCs photocatalysts for the degradation of pollutant.

Order	Pollutants	Photocatalyst	Light Source	Reactor	Mass of Catalyst (mg)	Concentration (ppm)	Irradiation Time (min)	Conversion (%)	Mol. Wt.	Photon Flux (mW cm <sup>-2</sup> )	Quantum Yield (%)	Reference
<b>A. Photocatalytic performances of GO-rGO semiconductor composites for dye degradation</b>												
<b>A-1. MB</b>												
1	MB	rGO-WO <sub>3</sub>	light source was a 150 W xenon lamp.	20 °C self-made Lab Solar gas photocatalysis system with external light irradiation	50	7	120	100	2278.4	NA	NA	[6]
2	MB	rGO-WO <sub>3</sub>	One 300 W PLS-SXE 300 xenon lamp	equipped with a $\lambda < 400$ nm cut-off filter	20	10	70	95	2247.4	NA	NA	[20]
3	MB	rGO/N-TiO <sub>2</sub>	Two 20 W black-lights with 352 nm (UV) and 545 nm (Visible)	NA	10	8.8	60	80 (UV) and 95 (Visible)	2123.6	NA	NA	[28]
4	MB	rGO/N-TiO <sub>2</sub>	one 500 W Xenon lamp > 400 nm	Quartz cell	50	8.8	160	100	2137.6	NA	NA	[31]
5	MB	rGO-ZnO	one 300 W Xe lamp with 420 nm	NA	80	18	70	100	2125.2	NA	NA	[39]
6	MB	rGO-ZnO	one 500 W mercury lamp	NA	20	10	90	100	2125.2	NA	NA	[40]
7	MB	GO/CoFe <sub>2</sub> O <sub>4</sub> /CdS	one 40 W daylight lamp	NA	25	20	180	100	2422.8	NA	NA	[44]
8	MB	rGO-CoFe <sub>2</sub> O <sub>4</sub>	one 800 W Xe lamp	NA	10	20	180	100	2278.4	NA	NA	[45]
9	MB	rGO-CoFe <sub>2</sub> O <sub>4</sub>	A 100 W reading lamp	installed glass cut-off filter	25	10	75	90	2278.4	NA	NA	[46]
10	MB	rGO-ZnFe <sub>2</sub> O <sub>4</sub>	one 500 W xenon lamp > 420 nm	Glass reactor (100 mL)	50	10	90	61	2284.7	NA	NA	[51]
11	MB	rGO-ZnFe <sub>2</sub> O <sub>4</sub>	one 530 W lamp with >400 nm	Pyrex glass tube (100 mL)	25	10	120	100	2284.7	NA	NA	[54]
12	MB	NiFe <sub>2</sub> O <sub>4</sub> -GO	One 300 W UV-visible lamp	Quartz glass (100 mL)	100	20	600	90	2280.2	NA	NA	[56]
13	MB	MnFe <sub>2</sub> O <sub>4</sub> -GO	one 500 W mercury and xenon lamp	Glass tube (100 mL)	25	20	360	98	2274	NA	NA	[58]

Table 2. Cont.

Order	Pollutants	Photocatalyst	Light Source	Reactor	Mass of Catalyst (mg)	Concentration (ppm)	Irradiation Time (min)	Conversion (%)	Mol. Wt.	Photon Flux (mW cm <sup>-2</sup> )	Quantum Yield (%)	Reference
<b>A-2. MO</b>												
14	MO	rGO_Co <sub>3</sub> O <sub>4</sub>	One 100 W Xenon lamp	NA	10	30	180	80	2287	NA	NA	[21]
15	MO	rGO-TiO <sub>2</sub>	one 150 W medium-pressure mercury vapor lamp with >350 nm	quartz cylindrical reactor (7.5 mL)	100	500	30	100	2123.6	6	NA	[30]
16	MO	rGO-CoFe <sub>2</sub> O <sub>4</sub>	one 800 W Xe lamp	NA	10	20	180	25	2278.4	NA	NA	[45]
17	MO	rGO-CoFe <sub>2</sub> O <sub>4</sub>	A 100 W reading lamp	installed glass cut-off filter	25	10	75	60	2278.4	NA	NA	[46]
<b>A-3. RhB</b>												
18	RhB 6G	FGS/ZnO	Two 100 and 250 W high-pressure mercury lamps with 300 nm	Pyrex glass tube (1000 mL)	10	10	100	100	2125.2	NA	NA	[36]
19	RhB	rGO-CoFe <sub>2</sub> O <sub>4</sub>	one 800 W Xe lamp	NA	10	20	180	75	2278.4	NA	NA	[45]
20	RhB	rGO-CoFe <sub>2</sub> O <sub>4</sub>	A 100 W reading lamp	installed glass cut-off filter	25	10	75	90	2278.4	NA	NA	[46]
21	RhB	rGO-Bi <sub>2</sub> WO <sub>6</sub>	one 500 W Xe lamp with 420 nm	Installed glass cut-off filter to visible-light irradiation glass tube (500 mL)	100	0.355	15	98	2740.8	NA	NA	[59]
<b>B. Photocatalytic performances of GO-rGO semiconductor composites for organic pollutants degradation</b>												
22	sulfamethoxazole	rGO-WO <sub>3</sub>	200 W Xe arc lamp with specific ranges 420–630 nm	1.5 AM solar simulator	10	20	180	100	2247	NA	NA	[18]
23	1-Naphthol	rGO-WO <sub>3</sub>	One Xe lamp 570 W	cylindrical Pyrex reactor of 7 cm diameter and 15 cm height	50	150	120	100	2247	NA	NA	[19]

Table 2. Cont.

Order	Pollutants	Photocatalyst	Light Source	Reactor	Mass of Catalyst (mg)	Concentration (ppm)	Irradiation Time (min)	Conversion (%)	Mol. Wt.	Photon Flux (mW cm <sup>-2</sup> )	Quantum Yield (%)	Reference
24	Chain chlorinated paraffin's	RGO/CoFe <sub>2</sub> O <sub>4</sub> /Ag	One 500 W xenon lamp with 400 nm	in situ quartz reaction cell	10	NA	720	90	2386.2	NA	NA	[49]
25	<sup>17</sup> α-ethinylestradiol	rGO/ZnFe <sub>2</sub> O <sub>4</sub> -Ag	One 300 W Xe-lamp	NA	100	2	240	100	2382	NA	NA	[53]

Furthermore, the self-redox properties of iron and manganese atoms in  $\text{MnFe}_2\text{O}_4$  induced by  $\text{S}_2\text{O}_8^{2-}$  were particularly useful for the generation of  $\text{SO}_4^-$ . The quenching tests and electron spin resonance (ESR) display that  $h^+$ ,  $\text{O}^{2-}$ ,  $\text{SO}_4^-$ , and OH are accountable for decomposition of antibiotics. Overall, irrespective of other parameters, the solvothermal method is best and helps in crystal growing and super saturation is achieved by reducing the temperature in the crystal growth zone.

Further, noble metal (Ag, Au, Cu, etc.) exhibits surface plasmon resonance (SPR), which is a characteristic feature. The SPR frequency of the metal particles can be tuned into visible light absorption by shifting the size of the deposited metal particles on the catalyst. Deposited metal is involved in multiple crucial roles, such as serving as a passive electron sink with high capacity to store electrons to suppress photogenerated charge carrier recombination, facilitates rapid dioxygen reduction to generate free radicals and direct excitation of metals, especially under visible light, and vectorial electron transfer to the conduction band (CB) of metal oxide. Thereby, showing improvement in the photocatalysis for the removal of various organic pollutants/dyes.

#### 4. Perspectives and Challenges

Graphene nanosheets act as a substrate to support the metal oxides for photocatalytic activity and graphene-based semiconductor photocatalysts are used for environmental remediation. The morphologies of semiconductors, theoretical electronic-structure calculations, and experimental discovery determinations are necessary on GO to persuade the photocatalytic activity, and composition design is an operative method to enhance the photocatalytic properties. Photocatalytic properties depend on the preparative method, and various parameters like initial concentration, oxidant concentration, pH, particle size, number of GO sheets, and source of light should be explored.

The interface regulates the efficacy of the electron-hole separation. Currently, only few methods succeed in unswervingly depicting the interaction of GR and nanoparticles. Atomic force microscopy (AFM), Surface-enhanced Raman scattering (SERS), and scanning transmission electron microscope (STEM) may be the best techniques for determining the interaction of graphene and nanoparticles. Finally, studies on the preparation of a ternary composite as a photocatalyst for both UV and visible-light-driven pollutant photodegradation have been studied and reported. Especially, for the design of ternary composite, magnetic materials such as Fe, Co, Mn, etc., as a dopant, and possessing unique advantages, show a remarkable photocatalytic activity and photostability.

Further tasks exist in the application of graphene-based composite for the industrial scale. Some innovative applications of the metal oxide-graphene entail specific understanding between the metal oxides and surface of the graphene, which will have a direct impact on the properties of the composite. Designing a structure for the overall photocatalysis process may require further exploiting of GO by chemically modifying methods. A synthetic approach method of GO-based composite structure by using novel materials has not been achieved to date for photocatalysis, but the solutions to the key challenges appear within reach.

In view of this, graphene-based composites possess diverse potential applications, individually having dissimilar desires concerning material properties, and it can be projected that the research on graphene-composite materials will have an optimistic future.

**Author Contributions:** Conceptualization: S.M. (Soumen Mandal) and S.M. (Srinivas Mallapur); writing—original draft preparation: S.M. (Soumen Mandal), S.M. (Srinivas Mallapur), M.R., J.K.S., D.-E.L. and T.P.; writing—review and editing: S.M. (Soumen Mandal), S.M. (Srinivas Mallapur), M.R., J.K.S., D.-E.L. and T.P.; supervision: D.-E.L. and T.P.; funding acquisition: D.-E.L. and T.P. All authors have read and agreed to the published version of the manuscript.

**Funding:** This work was supported by the National Research Foundation of Korea (NRF) grant funded by the Ministry of Science and ICT (MSIT), Korea (No. NRF-2018R1A5A1025137).

**Conflicts of Interest:** The authors declare no conflict of interest.

## References

1. Deng, X.; Lü, L.; Li, H.; Luo, F. The adsorption properties of Pb(II) and Cd(II) on functionalized graphene prepared by electrolysis method. *J. Hazard. Mater.* **2010**, *183*, 923–930. [[CrossRef](#)] [[PubMed](#)]
2. Yang, S.-T.; Chang, Y.; Wang, H.; Liu, G.; Chen, S.; Wang, Y.; Liu, Y.; Cao, A. Folding/aggregation of graphene oxide and its application in Cu<sup>2+</sup> removal. *J. Colloid Interface Sci.* **2010**, *351*, 122–127. [[CrossRef](#)] [[PubMed](#)]
3. Zhang, N.; Qiu, H.; Si, Y.; Wang, W.; Gao, J. Fabrication of highly porous biodegradable monoliths strengthened by graphene oxide and their adsorption of metal ions. *Carbon* **2011**, *49*, 827–837. [[CrossRef](#)]
4. Yeh, T.-F.; Syu, J.-M.; Cheng, C.; Chang, T.-H.; Teng, H. Graphite Oxide as a Photocatalyst for Hydrogen Production from Water. *Adv. Funct. Mater.* **2010**, *20*, 2255–2262. [[CrossRef](#)]
5. Zhao, G.; Wen, T.; Chen, C.; Wang, X. Synthesis of graphene-based nanomaterials and their application in energy-related and environmental-related areas. *RSC Adv.* **2012**, *2*, 9286–9303. [[CrossRef](#)]
6. Li, F.; Tian, X.; Yuhong, Z.; Jun, Y.; Aiwu, W.; Zhong, W. Preparation of WO<sub>3</sub>-reduced graphene oxide nanocomposites with Enhanced Photocatalytic Property. *Ceram. Int.* **2015**, *41*, 5903–5908.
7. Lorestani, F.; Shahnava, Z.; Mn, P.; Alias, Y.; Manan, N.S.A. One-step hydrothermal green synthesis of silver nanoparticle-carbon nanotube reduced-graphene oxide composite and its application as hydrogen peroxide sensor. *Sens. Actuators B-Chem.* **2015**, *208*, 389–398. [[CrossRef](#)]
8. Yu, B.; Xu, J.; Liu, J.-H.; Yang, S.-T.; Luo, J.; Zhou, Q.; Wan, J.; Liao, R.; Wang, H.; Liu, Y. Adsorption behavior of copper ions on graphene oxide-chitosan aerogel. *J. Environ. Chem. Eng.* **2013**, *1*, 1044–1050. [[CrossRef](#)]
9. Fu, Y.; Wang, J.; Liu, Q.; Zeng, H. Water-dispersible magnetic nanoparticle-graphene oxide composites for selenium removal. *Carbon* **2014**, *77*, 710–721. [[CrossRef](#)]
10. Li, B.; Liu, T.; Wang, Y.; Wang, Z. ZnO/graphene-oxide nanocomposite with remarkably enhanced visible-light-driven photocatalytic performance. *J. Colloid Interface Sci.* **2012**, *377*, 114–121. [[CrossRef](#)]
11. Wu, S.; Wang, P.; Cai, Y.; Liang, D.; Ye, Y.; Tian, Z.; Liu, J.; Liang, C. Reduced graphene oxide anchored magnetic ZnFe<sub>2</sub>O<sub>4</sub> nanoparticles with enhanced visible-light photocatalytic activity. *RSC Adv.* **2015**, *5*, 9069–9074. [[CrossRef](#)]
12. Tan, L.-L.; Chai, S.-P.; Mohamed, A.R. Synthesis and Applications of Graphene-Based TiO<sub>2</sub> Photocatalysts. *Chem. Sus. Chem.* **2012**, *5*, 1868–1882. [[CrossRef](#)] [[PubMed](#)]
13. Li, Y.; Du, Q.; Liu, T.; Peng, X.; Wang, J.; Sun, J.; Wang, Y.; Wu, S.; Wang, Z.; Xia, Y.; et al. Comparative study of methylene blue dye adsorption onto activated carbon, graphene oxide, and carbon nanotubes. *Chem. Eng. Res. Des.* **2013**, *91*, 361–368. [[CrossRef](#)]
14. Zhang, H.; Lv, X.; Li, Y.; Wang, Y.; Li, J. P25-Graphene Composite as a High Performance Photocatalyst. *ACS Nano* **2010**, *4*, 380–386. [[CrossRef](#)] [[PubMed](#)]
15. An, X.; Yu, J.C. Graphene-based photocatalytic composites. *RSC Adv.* **2011**, *1*, 1426–1434. [[CrossRef](#)]
16. Du, J.; Lai, X.; Yang, N.; Zhai, J.; Kisailus, D.; Su, F.; Wang, D.; Jiang, L. Hierarchically Ordered Macro-Mesoporous TiO<sub>2</sub>-Graphene Composite Films: Improved Mass Transfer, Reduced Charge Recombination, and Their Enhanced Photocatalytic Activities. *ACS Nano* **2011**, *5*, 590–596. [[CrossRef](#)] [[PubMed](#)]
17. Wang, D.; Choi, D.; Li, J.; Yang, Z.; Nie, Z.; Kou, R.; Hu, D.; Wang, C.; Saraf, L.V.; Zhang, J.; et al. Self-Assembled TiO<sub>2</sub>-Graphene Hybrid Nanostructures for Enhanced Li-Ion Insertion. *ACS Nano* **2009**, *3*, 907–914. [[CrossRef](#)]
18. Wenyu, Z.; Faqian, S.; Ronn, G.; Yan, Z. Facile fabrication of RGO-WO<sub>3</sub> composites for effective visible light photocatalytic degradation of sulfamethoxazole. *Appl. Catal. B* **2017**, *207*, 93–102.
19. Hajishafiee, H.; Sangpour, P.; Tabrizi, N.S. Facile Synthesis and Photocatalytic Performance of WO<sub>3</sub>/rGO Nanocomposite for Degradation of 1-Naphthol. *Nano* **2015**, *10*, 1550072. [[CrossRef](#)]
20. Hu, X.; Xu, P.; Gong, H.; Yin, G. Synthesis and characterization of WO<sub>3</sub>/Graphene nanocomposites for enhanced photocatalytic activities by one-step in-situ hydrothermal reaction. *Materials* **2018**, *11*, 147.
21. Wang, W.; Levi, G.; Tade, M.O.; Li, Q. April. Evaluation of Photocatalytic Activity of Co<sub>3</sub>O<sub>4</sub>/Graphene Composite. In *2015 International Conference on Materials, Environmental and Biological Engineering*; Atlantis Press: Paris, France, 2015; pp. 561–564.

22. Pervaiz, E.; Liu, H.; Yang, M. Facile synthesis and enhanced photocatalytic activity of single-crystalline nanohybrids for the removal of organic pollutants. *Nanotechnology* **2017**, *28*, 105701. [[CrossRef](#)] [[PubMed](#)]
23. Yao, Y.; Yang, Z.; Sun, H.; Wang, S. Hydrothermal synthesis of Co<sub>3</sub>O<sub>4</sub>-graphene for heterogeneous activation of peroxymonosulfate for decomposition of phenol. *Ind. Eng. Chem. Res.* **2012**, *51*, 14958–14965. [[CrossRef](#)]
24. Štengl, V.; Bakardjieva, S.; Grygar, T.M.; Bludská, J.; Kormunda, M. TiO<sub>2</sub>-graphene oxide nanocomposite as advanced photocatalytic materials. *Chem. Cent. J.* **2013**, *7*, 41. [[CrossRef](#)] [[PubMed](#)]
25. Zhang, Y.; Tang, Z.R.; Fu, X.; Xu, Y.J. TiO<sub>2</sub>-graphene nanocomposites for gas-phase photocatalytic degradation of volatile aromatic pollutant: Is TiO<sub>2</sub>-graphene truly different from other TiO<sub>2</sub>-carbon composite materials? *ACS Nano* **2010**, *4*, 7303–7314. [[CrossRef](#)] [[PubMed](#)]
26. Zhou, K.; Zhu, Y.; Yang, X.; Jiang, X.; Li, C. Preparation of graphene-TiO<sub>2</sub> composites with enhanced photocatalytic activity. *New J. Chem.* **2011**, *35*, 353–359. [[CrossRef](#)]
27. Anandan, S.; Narasinga Rao, T.; Sathish, M.; Rangappa, D.; Honma, I.; Miyauchi, M. Superhydrophilic graphene-loaded TiO<sub>2</sub> thin film for self-cleaning applications. *ACS Appl. Mater. Interfaces* **2013**, *5*, 207–212. [[CrossRef](#)]
28. Nguyen-Phan, T.D.; Pham, V.H.; Shin, E.W.; Pham, H.D.; Kim, S.; Chung, J.S.; Kim, E.J.; Hur, S.H. The role of graphene oxide content on the adsorption-enhanced photocatalysis of titanium dioxide/graphene oxide composites. *Chem. Eng. J.* **2011**, *170*, 226–232. [[CrossRef](#)]
29. Min, Y.; Zhang, K.; Zhao, W.; Zheng, F.; Chen, Y.; Zhang, Y. Enhanced chemical interaction between TiO<sub>2</sub> and graphene oxide for photocatalytic decolorization of methylene blue. *Chem. Eng. J.* **2012**, *193–194*, 203–210. [[CrossRef](#)]
30. Pastrana-Martínez, L.M.; Morales-Torres, S.; Likodimos, V.; Figueiredo, J.L.; Faria, J.L.; Falaras, P.; Silva, A.M. Advanced nanostructured photocatalysts based on reduced graphene oxide-TiO<sub>2</sub> composites for degradation of diphenhydramine pharmaceutical and methyl orange dye. *Appl. Catal. B* **2012**, *123*, 241–256. [[CrossRef](#)]
31. Yin, X.; Zhang, H.; Xu, P.; Han, J.; Li, J.; He, M. Simultaneous N-doping of reduced graphene oxide and TiO<sub>2</sub> in the composite for visible light photodegradation of methylene blue with enhanced performance. *RSC Adv.* **2013**, *3*, 18474–18481. [[CrossRef](#)]
32. Chacko, D.K.; Madhavan, A.A.; Arun, T.A.; Thomas, S.; Anjusree, G.S.; Deepak, T.G.; Balakrishnan, A.; Subramanian, K.R.V.; Sivakumar, N.; Nair, S.V.; et al. Ultrafine TiO<sub>2</sub> nanofibers for photocatalysis. *RSC Adv.* **2013**, *3*, 24858–24862. [[CrossRef](#)]
33. Linley, S.; Liu, Y.; Ptacek, C.J.; Blowes, D.W.; Gu, F.X. Recyclable Graphene Oxide-Supported Titanium Dioxide Photocatalysts with Tunable Properties. *ACS Appl. Mater. Interfaces* **2014**, *6*, 4658–4668. [[CrossRef](#)] [[PubMed](#)]
34. Maruthamani, D.; Divakar, D.; Kumaravel, M. Enhanced photocatalytic activity of TiO<sub>2</sub> by reduced graphene oxide in mineralization of Rhodamine B dye. *J. Ind. Eng. Chem.* **2015**, *30*, 33–43. [[CrossRef](#)]
35. Kim, C.H.; Kim, B.; Yang, K.S. TiO<sub>2</sub> nanoparticles loaded on graphene/carbon composite nanofibers by electrospinning for increased photocatalysis. In Proceedings of the 2nd International Symposium on Physics and Technology of Sensors (ISPTS), Pune, India, 7–10 March 2015.
36. Yang, Y.; Ren, L.; Zhang, C.; Huang, S.; Liu, T. Facile Fabrication of Functionalized Graphene Sheets (FGS)/ZnO Nanocomposites with Photocatalytic Property. *ACS Appl. Mater. Interfaces* **2011**, *3*, 2779–2785. [[CrossRef](#)]
37. Azarang, M.; Shuhaimi, A.; Yousefi, R.; Moradi Golsheikh, A.; Sookhajian, M. Synthesis and characterization of ZnO NPs/reduced graphene oxide nanocomposite prepared in gelatin medium as highly efficient photo-degradation of MB. *Ceram. Int.* **2014**, *40*, 10217–10221. [[CrossRef](#)]
38. Zhang, X.Y.; Li, H.P.; Cui, X.L.; Lin, Y. Graphene/TiO<sub>2</sub> nanocomposites: Synthesis, characterization and application in hydrogen evolution from water photocatalytic splitting. *J. Mater. Chem.* **2010**, *20*, 2801–2806. [[CrossRef](#)]
39. Li, B.; Cao, H. ZnO@graphene composite with enhanced performance for the removal of dye from water. *J. Mater. Chem.* **2011**, *21*, 3346–3349. [[CrossRef](#)]
40. Luo, Q.-P.; Yu, X.-Y.; Lei, B.-X.; Chen, H.-Y.; Kuang, D.-B.; Su, C.-Y. Reduced Graphene Oxide-Hierarchical ZnO Hollow Sphere Composites with Enhanced Photocurrent and Photocatalytic Activity. *J. Phys. Chem. C* **2012**, *116*, 8111–8117. [[CrossRef](#)]

41. Xitao, W.; Rong, L.; Kang, W. Synthesis of ZnO@ZnS-Bi<sub>2</sub>S<sub>3</sub> core-shell nanorod grown on reduced graphene oxide sheets and its enhanced photocatalytic performance. *J. Mater. Chem. A* **2014**, *2*, 8304–8313. [[CrossRef](#)]
42. Yao, Y.; Yang, Z.; Zhang, D.; Peng, W.; Sun, H.; Wang, S. Magnetic CoFe<sub>2</sub>O<sub>4</sub>-Graphene Hybrids: Facile Synthesis, Characterization, and Catalytic Properties. *Ind. Eng. Chem. Res.* **2012**, *51*, 6044–6051. [[CrossRef](#)]
43. Zhang, D.; Pu, X.; Gao, Y.; Su, C.; Li, H.; Li, H.; Hang, W. One-step combustion synthesis of CoFe<sub>2</sub>O<sub>4</sub>-graphene hybrid materials for photodegradation of methylene blue. *Mater. Lett.* **2013**, *113*, 179–181. [[CrossRef](#)]
44. Shi, Y.; Zhou, K.; Wang, B.; Jiang, S.; Qian, X.; Gui, Z.; Yuen, R.K.; Hu, Y. Ternary graphene-CoFe<sub>2</sub>O<sub>4</sub>/CdS nanohybrids: Preparation and application as recyclable photocatalysts. *J. Mater. Chem. A* **2014**, *2*, 535–544. [[CrossRef](#)]
45. He, G.; Ding, J.; Zhang, J.; Hao, Q.; Chen, H. One-Step Ball-Milling Preparation of Highly Photocatalytic Active CoFe<sub>2</sub>O<sub>4</sub>-Reduced Graphene Oxide Heterojunctions for Organic Dye Removal. *Ind. Eng. Chem. Res.* **2015**, *54*, 2862–2867. [[CrossRef](#)]
46. Moitra, D.; Chandel, M.; Ghosh, B.K.; Jani, R.K.; Patra, M.K.; Vadera, S.R.; Ghosh, N.N. A simple 'in situ' co-precipitation method for the preparation of multifunctional CoFe<sub>2</sub>O<sub>4</sub>-reduced graphene oxide nanocomposites: Excellent microwave absorber and highly efficient magnetically separable recyclable photocatalyst for dye degradation. *RSC Adv.* **2016**, *6*, 76759–76772. [[CrossRef](#)]
47. Suwanchawalit, C.; Somjit, V. Hydrothermal synthesis of magnetic CoFe<sub>2</sub>O<sub>4</sub>-graphene nanocomposite with enhanced photocatalytic performance. *Dig. J. Nanomater. Biostruct.* **2015**, *10*, 769–777.
48. Haw, C.; Chiu, W.; Abdul Rahman, S.; Khiew, P.; Radiman, S.; Abdul Shukor, R.; Hamid, M.A.A.; Ghazali, N. The design of new magnetic-photocatalyst nanocomposites (CoFe<sub>2</sub>O<sub>4</sub>-TiO<sub>2</sub>) as smart nanomaterials for recyclable-photocatalysis applications. *New J. Chem.* **2016**, *40*, 1124–1136. [[CrossRef](#)]
49. Chen, X.; Zhao, Q.; Li, X.; Wang, D. Enhanced photocatalytic activity of degrading short chain chlorinated paraffins over reduced graphene oxide/CoFe<sub>2</sub>O<sub>4</sub>/Ag nanocomposite. *J. Colloid Interface Sci.* **2016**, *479*, 89–97. [[CrossRef](#)]
50. Devi, L.G.; Srinivas, M. Hydrothermal synthesis of reduced graphene oxide-CoFe<sub>2</sub>O<sub>4</sub> heteroarchitecture for high visible light photocatalytic activity: Exploration of efficiency, stability and mechanistic pathways. *J. Environ. Chem. Eng.* **2017**, *5*, 3243–3255. [[CrossRef](#)]
51. Fu, Y.; Wang, X. Magnetically Separable ZnFe<sub>2</sub>O<sub>4</sub>-Graphene Catalyst and its High Photocatalytic Performance under Visible Light Irradiation. *Ind. Eng. Chem. Res.* **2011**, *50*, 7210–7218. [[CrossRef](#)]
52. Yang, D.; Feng, J.; Jiang, L.; Wu, X.; Sheng, L.; Jiang, Y.; Wei, T.; Fan, Z. Photocatalyst Interface Engineering: Spatially Confined Growth of ZnFe<sub>2</sub>O<sub>4</sub> within Graphene Networks as Excellent Visible-Light-Driven Photocatalysts. *Adv. Funct. Mater.* **2015**, *25*, 7080–7087. [[CrossRef](#)]
53. Khadgi, N.; Li, Y.; Upreti, A.R.; Zhang, C.; Zhang, W.; Wang, Y.; Wang, D. Enhanced Photocatalytic Degradation of 17 $\alpha$ -Ethinylestradiol Exhibited by Multifunctional ZnFe<sub>2</sub>O<sub>4</sub>-Ag/rGO Nanocomposite Under Visible Light. *Photochem. Photobiol.* **2016**, *92*, 238–246. [[CrossRef](#)] [[PubMed](#)]
54. Jenita Rani, G.; Jothi Rajan, M.A.; Gnana kumar, G. Reduced graphene oxide/ZnFe<sub>2</sub>O<sub>4</sub> nanocomposite as an efficient catalyst for the photocatalytic degradation of methylene blue dye. *Res. Chem. Intermed.* **2017**, *43*, 2669–2690. [[CrossRef](#)]
55. Fu, Y.; Chen, H.; Sun, X.; Wang, X. Graphene-supported nickel ferrite: A magnetically separable photocatalyst with high activity under visible light. *AIChE J.* **2012**, *58*, 3298–3305. [[CrossRef](#)]
56. Liu, S.-Q.; Xiao, B.; Feng, L.-R.; Zhou, S.-S.; Chen, Z.-G.; Liu, C.-B.; Chen, F.; Wu, Z.-Y.; Xu, N.; Oh, W.-C.; et al. Graphene oxide enhances the Fenton-like photocatalytic activity of nickel ferrite for degradation of dyes under visible light irradiation. *Carbon* **2013**, *64*, 197–206. [[CrossRef](#)]
57. Zeng, J.; Song, T.; Lv, M.; Wang, T.; Qin, J.; Zeng, H. Plasmonic photocatalyst Au/g-C<sub>3</sub>N<sub>4</sub>/NiFe<sub>2</sub>O<sub>4</sub> nanocomposites for enhanced visible-light-driven photocatalytic hydrogen evolution. *RSC Adv.* **2016**, *6*, 54964–54975. [[CrossRef](#)]
58. Fu, Y.; Xiong, P.; Chen, H.; Sun, X.; Wang, X. High Photocatalytic Activity of Magnetically Separable Manganese Ferrite-Graphene Heteroarchitectures. *Ind. Eng. Chem. Res.* **2012**, *51*, 725–731. [[CrossRef](#)]
59. Gao, E.; Wang, W.; Shang, M.; Xu, J. Synthesis and enhanced photocatalytic performance of graphene-Bi<sub>2</sub>WO<sub>6</sub> composite. *Phys. Chem. Chem. Phys.* **2011**, *13*, 2887–2893. [[CrossRef](#)]

60. Li, Z.; Shen, Y.; Yang, C.; Lei, Y.; Guan, Y.; Lin, Y.; Liu, D.; Nan, C.-W. Significant enhancement in the visible light photocatalytic properties of BiFeO<sub>3</sub>–graphene nanohybrids. *J. Mater. Chem. A* **2013**, *1*, 823–829. [[CrossRef](#)]
61. Lee, S.; Amaranatha Reddy, D.; Kim, T.K. Well-wrapped reduced graphene oxide nanosheets on Nb<sub>3</sub>O<sub>7</sub>(OH) nanostructures as good electron collectors and transporters for efficient photocatalytic degradation of rhodamine B and phenol. *RSC Adv.* **2016**, *6*, 37180–37188. [[CrossRef](#)]

**Publisher’s Note:** MDPI stays neutral with regard to jurisdictional claims in published maps and institutional affiliations.



© 2020 by the authors. Licensee MDPI, Basel, Switzerland. This article is an open access article distributed under the terms and conditions of the Creative Commons Attribution (CC BY) license (<http://creativecommons.org/licenses/by/4.0/>).